Naunyn-Schmiedeberg's Archives of Pharmacology (2023) 396:925–937
https://doi.org/10.1007/s00210-022-02361-w

RESEARCH

Coumaric acid from *M. polymorphum* extracts reverses the activated state of hepatic stellate cells (GRX) and inhibits their proliferation by decreasing the p53/p21 pathway

Matheus Scherer Bastos[1,2] · Rafaela Mallmann Saalfeld[1] · Bruna Pasqualotto Costa[1] · Krist Helen Antunes[3] · Denizar Melo[1] · Márcio Vinicius Fagundes Donadio[1,4] · Eliane Romanato Santarém[2] · Jarbas Rodrigues de Oliveira[1]

Received: 11 August 2022 / Accepted: 5 December 2022 / Published online: 15 December 2022

Abstract

Coumaric acid is a phenolic compound found in medicinal plants. Its use has been reported in the treatment of inflammatory diseases, prevention of alterations induced by oxidative stress, as well as acetaminophen-induced hepatotoxicity. Thus, this study evaluated coumaric acid as a potential treatment for liver fibrosis. Cell proliferation was assessed by the trypan blue exclusion technique and the cytotoxicity of coumaric acid was performed using an LDH assay. Mechanisms of cell apoptosis were evaluated by flow cytometry. The expression of genes associated with apoptosis, cell cycle control, and fibrosis was assessed by qPCR. The production of lipid droplets was quantified by oil red staining. The experiments performed showed that the treatment with coumaric acid was able to reduce cell proliferation without causing cell cytotoxicity or apoptosis. Coumaric acid was able to inhibit the expression of cyclin D1 and CDK's (CDK2, CDK4, and CDK6), increasing p53 and p21, which could lead to cell cycle arrest. Treatment with coumaric acid was also able to revert the activated phenotype of GRX cells to their quiescent state. Thus, our results suggest that coumaric acid has a potential therapeutic effect against liver fibrosis.

Keywords Cell cycle arrest · Phenolic compounds · CDKI's · Phenotypic reversal

Abbreviations

α-SMA	Alpha smooth muscle actin
CA	Coumaric acid
CCND1	Cyclin D1
CDK's	Kinase-dependent cyclins
CDKI's	Kinase-dependent cyclins inhibitors
CIS	Cisplatin
CLA	Chlorogenic acid
CLI	Chronic liver injury
Col-1	Collagen
DMEM	Dulbecco's Modified Eagle's Medium
EMC	Extracellular matrix
F1	Fractions 1
F2	Fractions 2
F3	Fractions 3
FBS	Fetal bovine serum
GA	Gallic acid

✉ Matheus Scherer Bastos
matheus.bastos@acad.pucrs.br

Rafaela Mallmann Saalfeld
rafaelamallmann@terra.com.br

Bruna Pasqualotto Costa
bruna.pasqualotto@acad.pucrs.br

Krist Helen Antunes
krist_helen@hotmail.com

Denizar Melo
DMelo@pucrs.br

Márcio Vinicius Fagundes Donadio
mdonadio@pucrs.br

Eliane Romanato Santarém
esantarem@pucrs.br

Jarbas Rodrigues de Oliveira
jarbas@pucrs.br

[1] Laboratório de Biofísica Celular e Inflamação, Pontifícia Universidade Católica do Rio Grande do Sul (PUCRS), 6681 Ipiranga Ave., RS 90619-900 Porto Alegre, Brazil

[2] Laboratório de Biotecnologia Vegetal, PUCRS, Porto Alegre, Brazil

[3] Laboratório de Imunologia Clínica e Experimental, PUCRS, Porto Alegre, Brazil

[4] Department of Physiotherapy, Universitat Internacional de Catalunya (UIC), Barcelona, Spain

GFAP	Glial fibrillary acidic protein
GRX	Hepatic stellate cell line
HA	Hydroxybenzoic acid
HF	Hepatic fibrosis
HPLC	High-performance liquid chromatography
HSCs	Hepatic stellate cells
LDH	Lactate dehydrogenase
MP	*Moquiniastrum polymorphum subsp. Polymorphum*
NAC	N-acetylcysteine
PPAR-γ	Proliferation-activated gamma receptor
ORO	Oil red-O
TE	Total extract
TGF-β	Transforming growth factor beta

Introduction

Hepatic fibrosis (HF) is a regenerative process (Khomich et al. 2019) induced by chronic liver injury (CLI), representing an early stage in the progression to liver cirrhosis, hepatocellular carcinoma and, eventually, liver failure (Cheng et al. 2021). Unlike acute liver injury, which allows the organ to recover all its original mass and architecture, CLI is triggered by different etiologies, inducing repetitive tissue injury, resulting in an impaired regenerative capacity and marked by an altered inflammatory infiltrate, leading to a chronic wound healing response (Ginès et al. 2021).

The main causes of liver fibrosis are schistosomiasis, viral hepatitis (hepatitis B and C), alcoholic liver disease, non-alcoholic fatty liver disease, as well as cholestatic and autoimmune liver diseases (Weiskirchen and Tacke 2016; Zhang et al. 2016; Higashi et al. 2017; Ginès et al. 2021). During HF, hepatic stellate cells (HSCs) acquire fibrogenic properties (activated phenotype), thus losing their intracellular lipid droplets and presenting characteristics of myofibroblasts. This mechanism promotes the accumulation of extracellular matrix (EMC) components, such as collagen (Col-1), alpha smooth muscle actin (α-SMA), desmin, and glial fibrillary acidic protein (GFAP) resulting in impaired liver function, deposition of fibrous scars, and, in more severe cases, liver cirrhosis accompanied by liver failure (Tsochatzis et al. 2014; Kisseleva and Brenner 2021).

Prior to their activation, HSCs remain in a non-proliferative, retinoid-storing state, also known as a quiescent state (Higashi et al. 2017). This is maintained by transcription factors, such as the peroxisome proliferation-activated gamma receptor (PPAR-γ), considered one of the key factors for the regulation of adipogenesis in HSCs, as well as for the regression of HF (Liu et al. 2020).

The treatment of HF aims to reduce or even reverse the fibrotic state, mainly by the activation of anti-inflammatory processes, inhibition of the proliferation and activation of HSCs, as well as decrease of the production and deposition of EMC. Currently, antioxidants such as vitamin E, silymarin, phosphatidylcholine, and S-adenosyl-L-methionine, are able to inhibit HSC activation and attenuate liver fibrosis. Moreover, transforming growth factor beta (TGF-β) inhibitors prevent scar formation in experimental liver fibrosis. N-acetylcysteine (NAC) is also another drug with antioxidant effects, being widely used for liver regeneration in patients intoxicated with paracetamol, managing to balance the hepatic values of glutathione that were destabilized with the use of paracetamol (Tsochatzis et al. 2014; Plano et al. 2021).

Plant extracts present molecules with antioxidant and anti-inflammatory properties known as phenolic compounds, which are widely used for the treatment of various diseases. Among the plants that present these properties, *Moquiniastrum polymorphum subsp. polymorphum* (MP) extracts have been used in medicine for the treatment of inflammatory diseases of the respiratory tract, chronic diseases, and cancer (Piornedo et al. 2011; David et al. 2014; Martins et al. 2015; Limeiras et al. 2017; de Moraes Gonçalves et al. 2019; Guarneire et al. 2021). Coumaric acid (CA) is one of the several phenolic compounds that can be found in plant extracts. It is a common compound found in several medicinal herbs and it has been used in the treatment of inflammatory lung diseases caused by cigarette smoke, as well as inflammatory bowel diseases (Kim et al. 2018b). It has been also shown that its use may decrease macrophages in typical inflammatory diseases, preventing the induction of oxidative stress, as well as acetaminophen-induced hepatotoxicity (Cha et al. 2018; Lee et al. 2019; Roychoudhury et al. 2021).

Therefore, the antioxidant properties of CA may be of great importance in the development of new strategies to treat HF. For this reason, this study aimed to evaluate the antifibrotic effects of CA in GRX cells, an activated HSC cell line.

Material and methods

Chemical and reagents

Absolute ethyl alcohol 99.5%, methanol, and dichloromethane (SYNTH, São Paulo, Brazil) were used to prepare the extract and fractions. Pure standards of phenolic compounds were purchased from Sigma-Aldrich (St. Louis, USA). DMEM (Dulbecco's Modified Eagle's Medium), amphotericin B (Fungizone®), fetal bovine serum (FBS), penicillin–streptomycin (10,000 U/mL), 0.5% trypsin/EDTA solution and Trypan blue were obtained from Gibco Laboratories (Carlsbad, USA). The lactate dehydrogenase (LDH) kit was purchased from Labtest (Minas Gerais, Brazil). Annexin V-FITC and propidium iodide were provided by Quatro G (Porto Alegre, Brazil). Trizol™ was purchased

from Invitrogen (Massachusetts, USA) and the GoScript kit used to produce cDNA was purchased from Promega (São Paulo, Brazil). The oil-red dye used to stain the lipid droplets was purchased from Sigma-Aldrich (St. Louis, USA).

Collection, preparation, fractionation, and identification of the main components of the crude extract and its fractions

The specimen of *Moquiniastrum polymorphum subsp. Polymorphum* was collected in Mariana Pimentel, Rio Grande do Sul, Brazil (30° 21 ′09 ″S; 51° 34 ′59″ W; 119 m). Afterward, it was identified, authenticated, and deposited in the Herbarium of the Museum of Science and Technology at the Pontifical Catholic University of Rio Grande do Sul-PUCRS (Herbarium MPUC; MPUC 22,565). Its leaves were dried, ground, and soaked in ethanol (80%), and filtered to prepare the total extract (TE). TE was fractionated on a silica chromatography column (stationary phase) and its mobile phases consisted of solutions of dichloromethane/methanol (90:10; v/v), methanol (100%), and methanol/water (80:20; v /v), resulting in fractions F1, F2, and F3, respectively. The TE and fractions (F1, F2, and F3) were dried under reduced pressure and then dissolved in DMEM at a concentration of 100 mg/mL (Basso et al. 2019). The profile of TE phenolic compounds and their fractions was analyzed by High-Performance Liquid Chromatography (HPLC), on a Sikam Chromatography™ S600, and UV–VIS Mod detector 3345DAD set at 280 nm. The separation of phenolic compounds was carried out on a MetaSil ODS column (5 µm; 250×4.6 mm), with a C18 guard column, in a 25 °C oven. The results obtained were analyzed using the Clarity Chromatography software. The molecules present in the extract were compared for retention times to commercial standards: coumaric acid (CA), gallic acid (GA), hydroxybenzoic acid (HA), and chlorogenic acid (CLA). The mobile phase consisted of methanol (eluent A) and acidic water with formic acid (2.5%; v/v) (eluent B). The linear gradient started with 10% eluent B from 0 to 10 min, 20 to 80% B from 10 to 25 min, 80 to 100% B from 25 to 32 min, and 100% B from 32 to 35 min, with a flow rate of 0.5 mL/min (Basso et al. 2019).

Cell culture, viability, and cytotoxicity

Activated hepatic stellate cell line (GRX; Bank of Cells of Rio de Janeiro; Brazil) was used for cell culture experiments. Cells were cultured in DMEM supplemented with 5% FBS, 0.1% (v/v) fungizone ® and 0.5 U/mL of penicillin/streptomycin, under 37 °C, 95% relative humidity and 5% CO_2 atmosphere. Cell viability was determined by the trypan blue exclusion assay (Strober 2001). GRX cells were seeded in a 24-well plate at 5×10^3 per well for 24 h and then treated with the phenolic compounds: CA (6.36 µg/mL), GA (0.24 µg/mL), HA (12.98 µg/mL) and CLA (1.62 µg/mL). After 72 h, cells were harvested and suspended in PBS containing trypan blue (1:1), and the amount of trypan blue positive cells was determined using a Neubauer chamber. The negative control consisted of cells treated with medium, while NAC (2.5 µg) was used as a positive control. Results are expressed as a percentage of live cells over the control group. The percentage of living cells was calculated using the following equation (Eq. 1). The evaluation of cytotoxicity was performed by the LDH enzymatic assay. The LDH assay is performed to assess a membrane disruption through cell necrosis (Kumar et al. 2018). GRX cells were seeded at 5×10^3 per well in 24-well plates and incubated with the phenolic compound CA (6.36 µg/mL) for 72 h. Enzyme activity was measured in the supernatant and cell lysate by colorimetry using the Lactate Dehydrogenase kit. Tween (5%) was used to control cell lysis. LDH release was measured at 490 nm on a microplate reader (EZ Read 400, Biochrom). In order to measure antiproliferative activity, the required concentration of TE and fractions (F1, F2, and F3) to inhibit the growth of HF by 50% (IC50) was calculated by plotting the percentage of relative cell viability (%) against the logarithm of the tested concentrations.

$$\%\ of\ living\ cells = \left(\frac{\mathrm{TBPC}_{Treated\ cells}}{Mean\ \mathrm{TBPC}_{Untreated\ cells}}\right)\times 100 \quad (1)$$

Cell death assay

The identification of living necrotic and apoptotic cells was performed by flow cytometry (FACS Canto II Flow Cytometer; Becton Dickinson, USA) as described by (Darzynkiewicz et al. 2001). GRX cells were seeded in a 24-well plate at a density of 5×10^3 cells per well and treated with CA (6.36 µg/mL). After 72 h, cells were harvested, washed with ice-cold PBS, resuspended in binding buffer (200 µL; 10 mM Hepes)/NaOH, pH 7.4, 140 mM NaCl, 2.5 mM CaCl2), 4 µL annexin V-FITC, 4 µL of propidium iodide (PI), and incubated at room temperature in the dark for 15 min. Untreated cells were used as a negative control and cells treated with 20 µM cisplatin (CIS) served as a positive control. Data were analyzed using FlowJo 7.6.5 software (Tree Star Inc., Ashland, OR).

Expression of profibrotic, apoptotic, senescent, and cell cycle arrest genes

The expression of genes related to fibrosis (TGF-β, Col-1, α-SMA, Desmin, and glial fibrillary acidic protein), lipid synthesis (PPAR-γ), apoptosis (BAX), CDKIs (p53, p21, p27, and p16), cyclin D1 and kinase-dependent cyclins (CDK2, CDK4, and CDK6) were assessed by real-time PCR. GRX cells were seeded at 10×10^4 cells per well in a six-well plate and cultured for 24 h. After that, the cells were treated with CA (6.36 µg/mL) for 72 h. Total RNA from controls and

treated GRX cells was extracted using Trizol and cDNA was synthesized using the GoScript reverse transcription kit, following the manufacturer's instructions. cDNA quantification was performed using NanoDrop 2000 (Thermo Fisher Scientific). A total of 64 ng of cDNA from each sample was used for the analysis of relative gene expression in quantitative real-time PCR (qPCR, Step One Plus–Applied Biosystems) using the SYBR green fluorescence marker (de Souza Basso et al. 2021). The relative expression of mRNA was calculated by the Delta-Delta Ct (ΔΔCt) method. B2M (mouse gene) was used as an internal control to normalize RNA variation. The primers used to assess gene expression are shown in Table 1. Samples were analyzed in duplicate.

Phenotypic reversion through the oil-red assay

Phenotypic reversion of hepatic stellate cells was observed using the oil red staining assay (Koopman et al. 2001). Cells were seeded in a 24-well cell culture plate, 3×10^3 cells/well, and treated with CA (6.36 µg/mL). After 72 h, cells were fixed with 10% formaldehyde for 1 h and then stained with Oil Red-O (ORO) (Sigma Chemical). After 30 min, intracellular lipid accumulation was observed using an inverted light microscope at 400 × magnification. For estimation of lipid accumulation, ORO within lipid droplets was extracted using isopropanol; absorbance was read at a wavelength of 492 nm using an ELISA plate reader. Specific lipid content was calculated as the ratio between the absorbance value obtained for ORO and the number of cell counts.

Statistical analysis

Results are expressed as mean ± standard error of the mean. Data were analyzed by one-way analysis of variance (ANOVA) followed by the Tukey posthoc test ($p < 0.05$). Statistical analyses were performed using the software GraphPad Prism 8.0.

Table 1 Sequence of primers used for qPCR

Gene	Primer sequences (5′–3′)	Reference
B2M	F: ACAGTTCCACCCGCCTCACATT	Stepanenko et al. (2022)
	R: TAGAAAGACCAGTCCTTGCTGAAG	
p53	F: TGCTCACCCTGGCTAAAGTT	Bassiony et al. (2014)
	R: AATGTCTCCTGGCTCAGAGG	
p16	F: TTGGCCCAAGAGCGGGGACA	Bassiony et al. (2014)
	R: GCGGGCTGAGGCCGGATTTA	
p21	F: CTGTCTTGCACTCTGGTGTCTGA-	Teratake et al. (2016)
	R: CCAATCTGCGCTTGGAGTGA	
p27	F: CAAAACCGAACAAAAGCGAAACGCCA	Teratake et al. (2016)
	R: GATACTCTCCCCTTCCTTTGCCTTGTC	
CCDN1	F: GCGTACCCTGACACCAATCTC	Teratake et al. (2016)
	R: ACTTGAAGTAAGATACGGAGGGC	
CDK2	F: ACCTCCCGCAGTGTTCCTATT	Teratake et al. (2016)
	R: CACAGACCTCTAGCATCCAGG	
CDK4	F: ACTGGCGCATCAGATCCTTA	Teratake et al. (2016)
	R: GGAGGCCTTTGAACATCCCA	
CDK6	F: GCTGACCAGCAGTACGAATG	Teratake et al. (2016)
	R: GCACACATCAAACAACCTGACC	
BAX	F: CTACAGGGTTTCATCCAG	Ghatei et al. (2017)
	R: CCAGTTCATCTCCAATTCG	
TGF-β	F: GGGAAATTGAGGGCTTTCGC	de Souza Basso et al. (2021)
	R: TGAACCCGTTGTCCACT	
Col-1	F: AGTGGTTTGGATGGTGCCAA	de Souza Basso et al. (2021)
	R: GCACCATCATTTCCACGAGC	
α-SMA	F: TAGCACCCAGCACCATGAAG	de Souza Basso et al. (2021)
	R: CTGCTGGAAGGTGGACAGAG	
PPAR-γ	F: CTACAGGGTTTCATCCAG	de Souza Basso et al. (2021)
	R: CCAGTTCATCTCCAATTCG	

Results

Evaluation of the effect of TE and fractions on cell proliferation

In order to evaluate the antiproliferative effect of the TE and its fractions, a concentration curve (60, 120, 250, 500, 1000, 2500, and 5000 µg/mL) was performed (Fig. 1). Results have shown that all concentrations presented significant antiproliferative action, with TE and F1 being the most pronounced effect (Table 2). IC50 values were obtained to compare the antiproliferative activity between TE, F1, F2, and F3. TE has shown antiproliferative activity with an IC50 value of 68.2 µg/mL, F1 showed an antiproliferative activity with an IC50 value of 59.7 µg/mL, F2 presented an IC50 value of 99.1 µg/mL, and F3 was able to decrease the number of cells, although it did not promote a 50% reduction in the cell population with the maximum concentration used (5000 µg/mL) (Fig. 1).

Table 2 Effect of extracts on cell proliferation at a concentration of 60 µg/mL

	% survive cell number
Control	100
TE	51
F1	50
F2	62
F3	90

Phytochemical analysis of *M. polymorphum* extracts and fractions

We have performed a chromatographic separation by HPLC (chromatogram is shown in Fig. 2) using a concentration of 60 µg/mL. The main phenolic compounds found and their retention times in the ethanol extract, as well as in the MP fractions are presented in Tables 3 and 4. The phytochemical analysis of the MP leaf extract showed the presence of CA, CLA, HA, and GA. The most abundant phenolic compounds for TE are HA and CA, while for the fractions, CA and CL were detected in F1. In F2, the most present was the CLA, although the GA was also detected. F3 contained only GA. Considering these results, the amounts found of each phenolic compound were used to test cell proliferation.

Evaluation of the effect of phenolic compounds in the proliferation of GRX cells

In order to assess the effect of molecules from extracts on the proliferation of GRX cells, we have used the highest concentrations found, according to Table 4. The treatment performed with HA and CLA at concentrations of 12.96 and 45.36 µg/mL did not show significant results

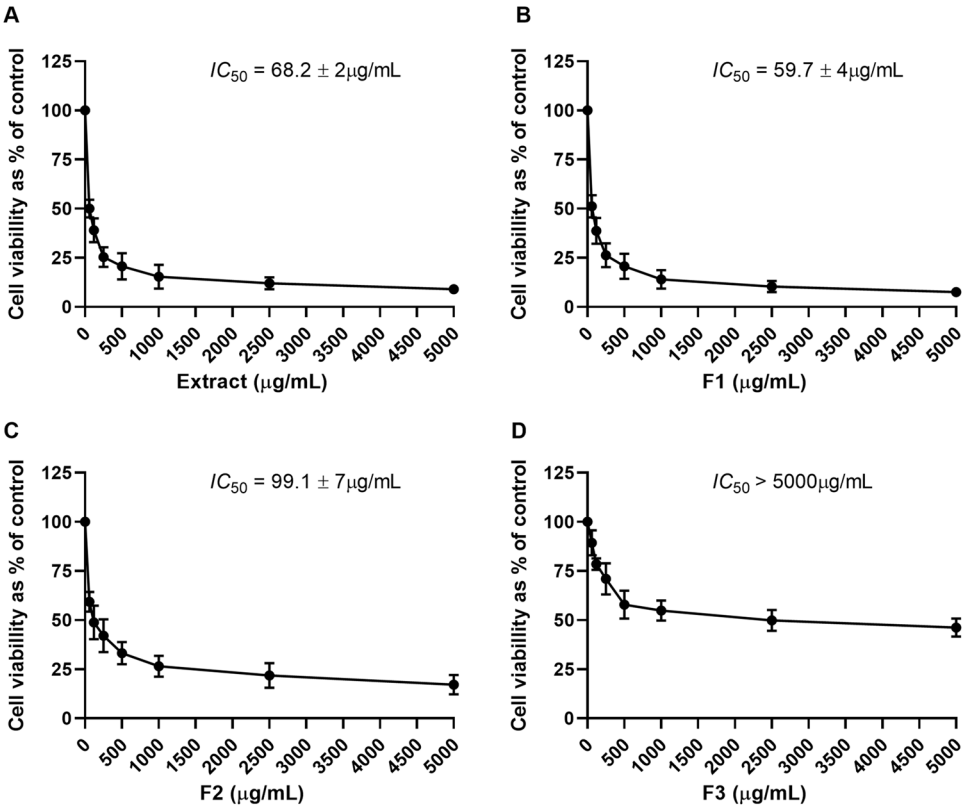

Fig. 1 Total extract concentrations and their fractions responsible for inhibiting 50% (IC50) of the relative cell viability. **A** Total extract, **B** F1, **C** F2, and **D** F3 at concentrations of 60, 125, 250, 500, 1000, 2500, and 5000 µg/mL. Cell proliferation was evaluated by the trypan blue exclusion method

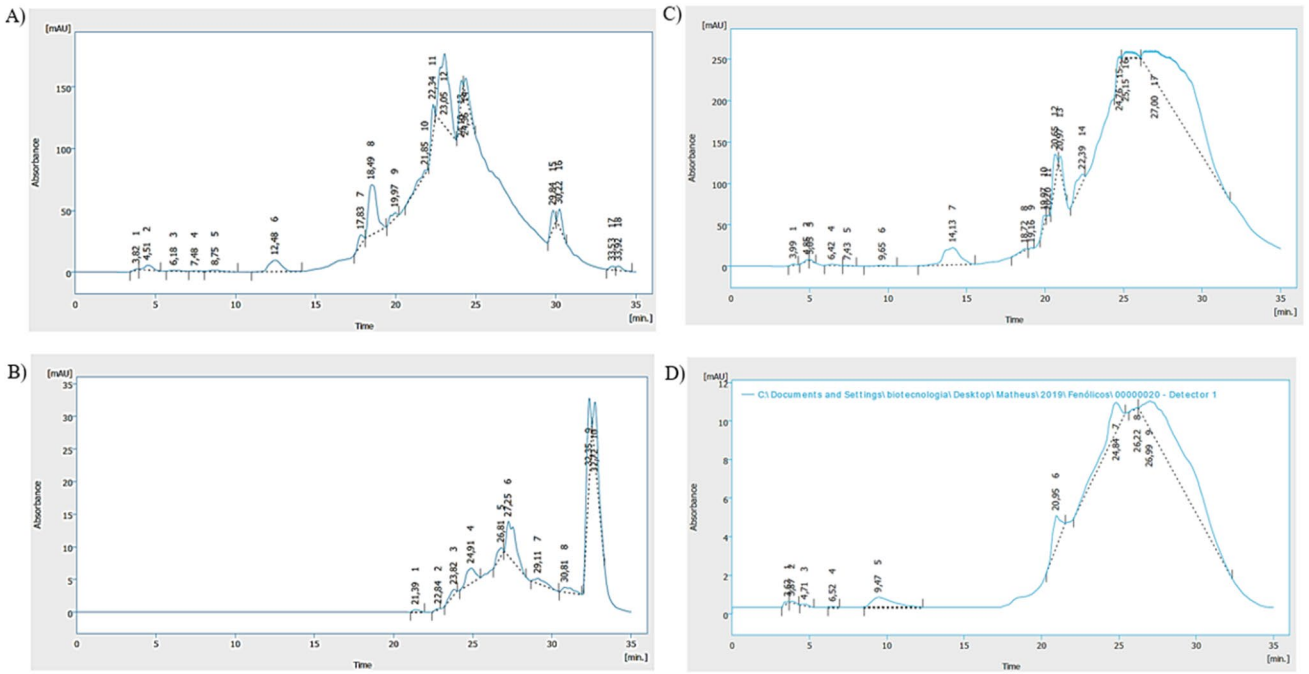

Fig. 2 HPLC analysis of phenolic compounds in the *M. polymorphum* obtained fractions. **A** TE, **B** F1, **C** F2, and **D** F3

Table 3 Retention time of the main phenolic compounds detected by HPLC in the extracts of *Moquiniastrum polymorphum* at a concentration of 60 µg/mL

Phenolic compounds	Retention time (min)				Compounds (%)			
	TE	F1	F2	F3	TE	F1	F2	F3
Hydroxybenzoic acid (HA)	18.49	ND	ND	ND	21.60%	ND	ND	ND
Coumaric acid (CA)	24.36	24.90	ND	ND	4.50%	10.60%	ND	ND
Chlorogenic acid (CLA)	21.85	21.39	27.00	ND	2.70%	1.30%	75.60%	ND
Gallic acid (GA)	3.82	ND	4.85	24.84	0.40%	ND	0.10%	16.30%

ND non-detected

Table 4 Concentration of the main phenolic compounds detected by HPLC in the extracts of *Moquiniastrum polymorphum* at a concentration of 60 µg/mL

Phenolic compounds	Concentration (60 µg/mL)			
	TE	FI	FII	FIII
Hydroxybenzoic acid (HA)	12.96 µg/60 µg	ND	ND	ND
Coumaric acid (CA)	2.70 µg/60 µg	6.36 µg/60 µg	ND	ND
Chlorogenic acid (CLA)	1.62 µg/60 µg	0.78 µg/60 µg	45.36 µg/60 µg	ND
Gallic acid (GA)	0.24 µg/60 µg	ND	0.06 µg/60 µg	9.78 µg/60 µg

ND non-detected

compared to the control group (Fig. 3). CA was able to inhibit proliferation by 36% at a concentration of 6.36 µg/mL, while GA decreased by 23% at a concentration of 9.78 µg/mL (Fig. 3). CA at 6.36 µg/mL was chosen as the phenolic compound for the following experiments since it presented the best effect among the phenolics obtained in the TE and fractions (Fig. 3).

Effect of CA on cellular cytotoxicity

Cell membrane integrity was assessed in order to rule out the possibility that the cellular decline of GRX cells during proliferation was associated with membrane damage. Treatment of cells with CA (6.36 µg/mL) did not result in a

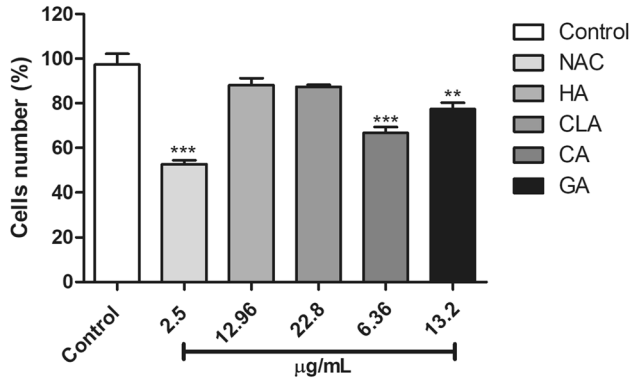

Fig. 3 Effect of phenolic compounds on cell proliferation after 72 h. NAC was used as a positive control (2.5 µg) to decrease proliferation. Cell proliferation was assessed by the trypan blue exclusion method. $^{**}p < 0.01$ and $^{***}p < 0.001$ compared to the control

significant release of LDH, which indicates no membrane damage in response to treatment (Fig. 4).

Effect of CA on apoptosis

In order to further investigate the mechanism leading to reduced cell proliferation, we have evaluated the process of cell death by apoptosis. There was no significant difference between CA and the negative control, both for total apoptosis and necrosis. On the other hand, the CIS (20 µM) positive control showed induction of apoptosis, as well as necrosis (Fig. 5A–B). In addition, to confirm these results, we have evaluated the BAX gene, which is a pro-apoptotic gene. Data have shown that there was no increase in the expression of the BAX gene (Fig. 5C), confirming that the treatment did not induce apoptosis and suggesting another path to decrease cell proliferation.

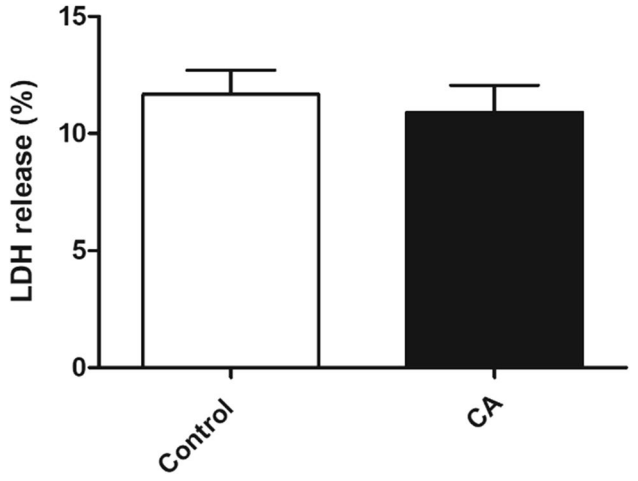

Fig. 4 The cytotoxicity of CA (6.36 µg/mL) was assessed by measuring the levels of LDH released. Data represent mean ± SD ($n = 4$). Results were expressed as a percentage of cells

Effect of CA on the expression of CDK inhibitor genes

Seeking to additionally examine the GRX cells' decrease in proliferation, we investigated the gene expression of CDKIs (CDKs inhibitors). There are two well-known families of CDKI's, the p53, p21, p27, and p57 (CIP/KIP inhibitors), and the p16, p15, p18, and p19 (INK4 inhibitors). The p53, p21, p27 genes (CIP/KIP inhibitors), and p16 (INK4 inhibitors) were measured and results have shown that p53 expression increased in response to CA treatment (Fig. 6A), which consequently induced the expression of the p21 gene (Fig. 6B). The p16 and p27 genes were not altered with the treatments tested (Fig. 6C–D).

Effect of CA on the expression of CDK genes

Considering the increase found in the expression of CDKI's p53 and p21, we have investigated the effect of CA on cyclin D1 and CDK's (kinase-dependent cyclins). Therefore, the expression of CCND1 (cyclin D1), as well as CDK2, CDK4, and CDK6 genes were evaluated. Results have demonstrated a decrease in CCND1 gene expression (Fig. 7A), as well as CDK2, CDK4, and CDK6 (Fig. 7B–D), demonstrating that treatment with CA may cause cell cycle arrest by downregulating cyclin D1 and CDK's.

Effect of CA on the phenotypic reversal of activated GRX cells

There are two possible ways to reduce liver fibrosis: (i) decreasing cell proliferation and (ii) reversing its activated phenotype. For this reason, we have examined the capacity of CA to reverse the activated GRX cell phenotype. Cells were evaluated by the red-o oil (ORO) technique and treatment with CA-induced GRX cells to increase fat storage in the cytoplasm (Fig. 8A–C). NAC treatment (positive control) also induced the accumulation of lipids in the cytoplasm (Fig. 8A–C). Since ORO staining showed the formation of fat droplets, the expression of PPAR-γ, which is a gene related to lipid synthesis, was evaluated. CA induced a significant increase in PPAR-γ mRNA expression, suggesting its involvement in the accumulation of lipid droplets in the cytoplasm of GRX cells (Fig. 8B).

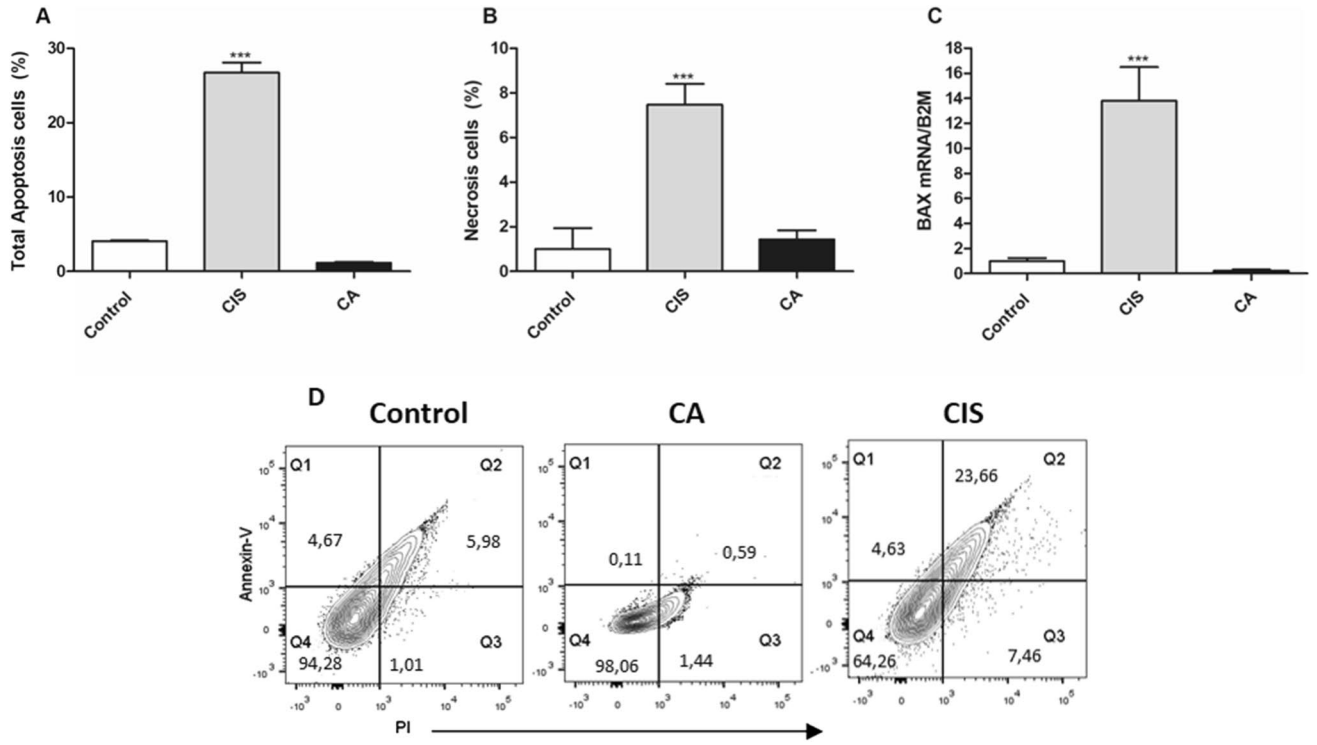

Fig. 5 Effect of CA on cell apoptosis. Cells were exposed to CA (6.36 µg/mL) and analyzed for **A** total apoptosis and **B** necrosis by flow cytometry. Cisplatin (20 µM) was used as a positive control. **C** Effect of CA on the BAX gene expression (pro-apoptotic) in GRX cells after 72 h of treatment. B2M was used as an internal control. **D** Representative flow cytometry plots of PI (*x*-axis)/Annexin (*y*-axis). Results are expressed as the percentage of apoptotic cells. Data represent mean ± SD ($n = 4$). ***$p < 0.001$ in comparison to the control (medium and cells)

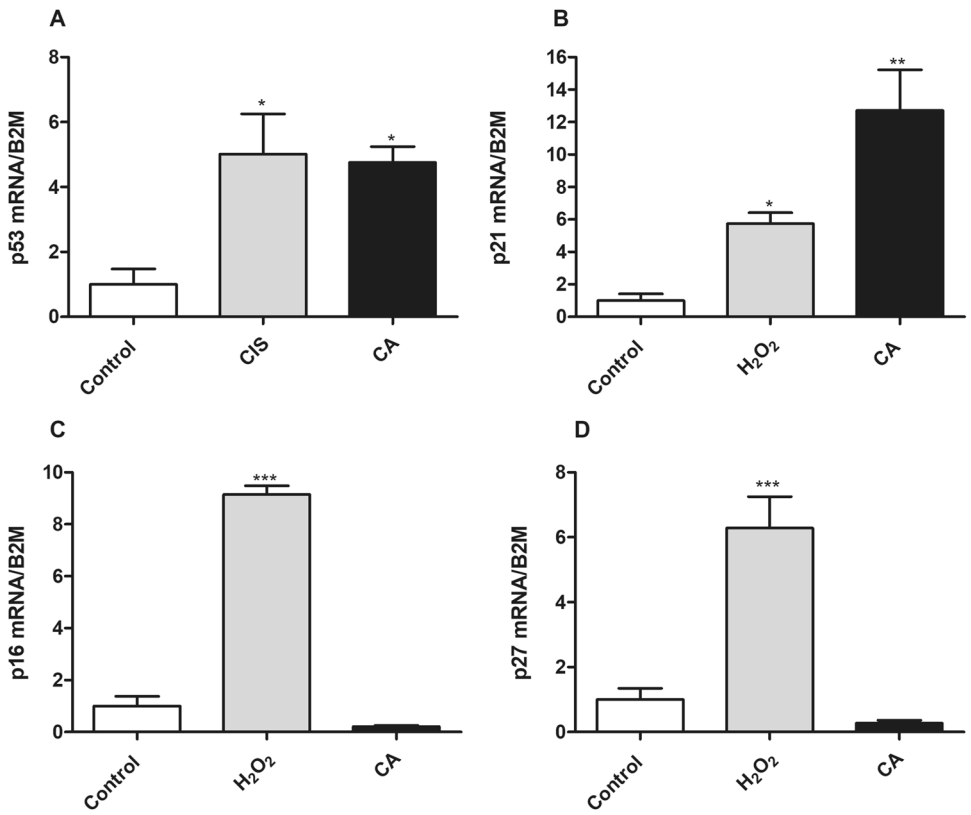

Fig. 6 Effect of CA on the expression of genes encoding cell growth regulators in GRX cells after 72 h of treatment. Relative expression of mRNA **A** p53, **B** p21, **C** p16, and **D** p27 in the treatment groups. B2M was used as an internal control. Results are expressed as target gene/B2M, and data represent mean ± SD ($n = 4$). *$p < 0.05$, **$p < 0.01$, and ***$p < 0.001$ in comparison to the control

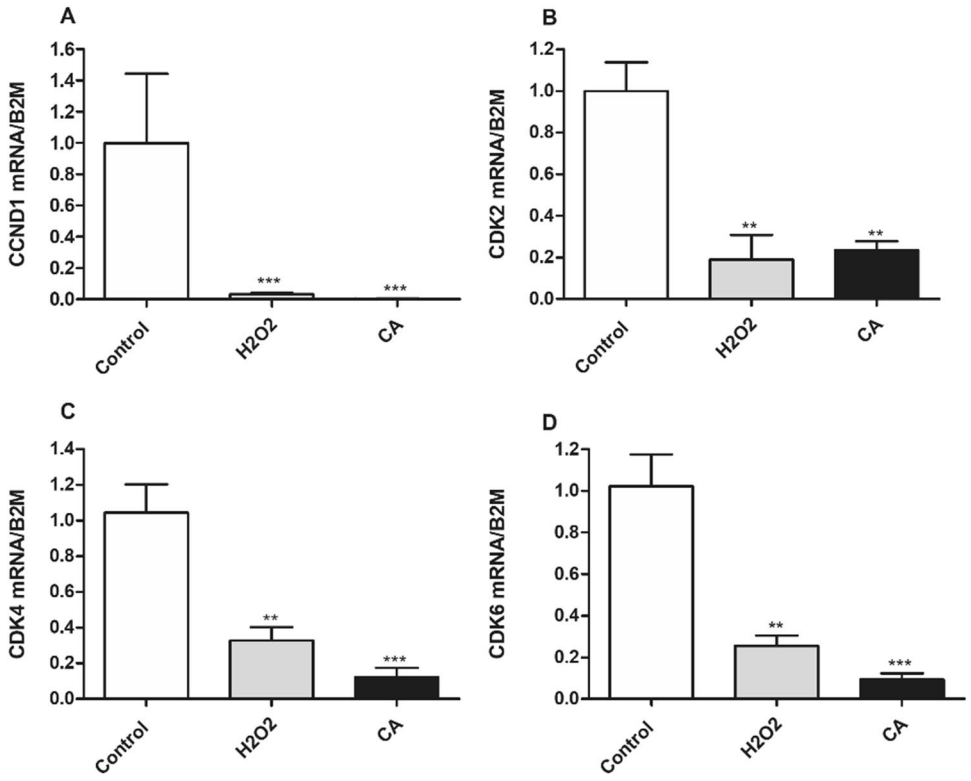

Fig. 7 Effect of CA on the expression of genes encoding cell cycle progression in GRX cells after 72 h of treatment. Relative expression of **A** CCND1, **B** CDK2, **C** CDK4, and **D** CDK6 mRNA in the treatment groups. B2M was used as an internal control. Results are expressed as target gene/B2M, and data represent mean ± SD ($n = 4$). $^{**}p < 0.01$ and $^{***}p < 0.001$ in comparison to the control

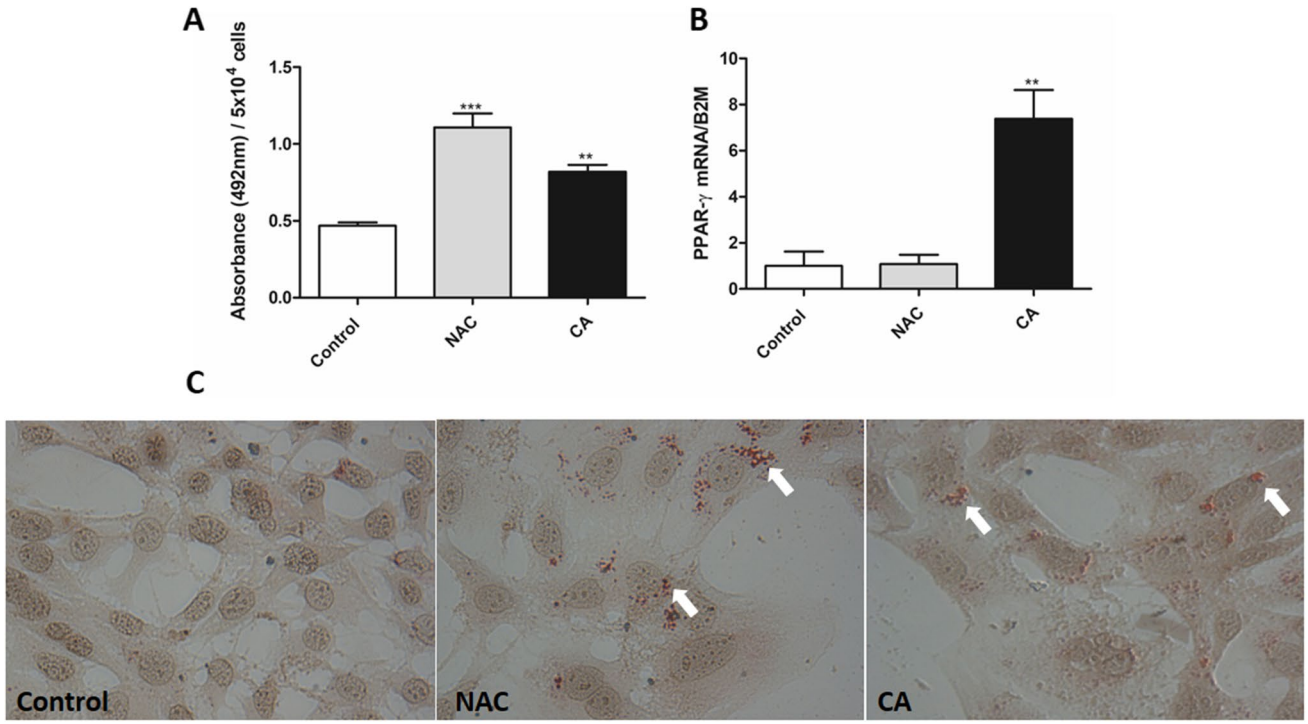

Fig. 8 Quantification of lipid droplets and 72 h-treated PPAR-γ mRNA expression. **A** Quantitative evaluation of CA treatment performed by quantification of lipid droplets dissolved in isopropyl alcohol (active absorbance for ORO adjusted for cell number 5×10^4). NAC was used as a positive control (2.5 µg). **C** Qualitative evaluation of lipid droplets stained with OIL-Red (400× magnification). Lipid droplets are indicated by arrows. **B** CA effect on 72 h-treated PPARγ mRNA expression. Results are expressed as target gene/B2M, and data represent mean ± SD ($n = 4$). $^{**}p < 0.01$ and $^{***}p < 0.001$ compared to the control

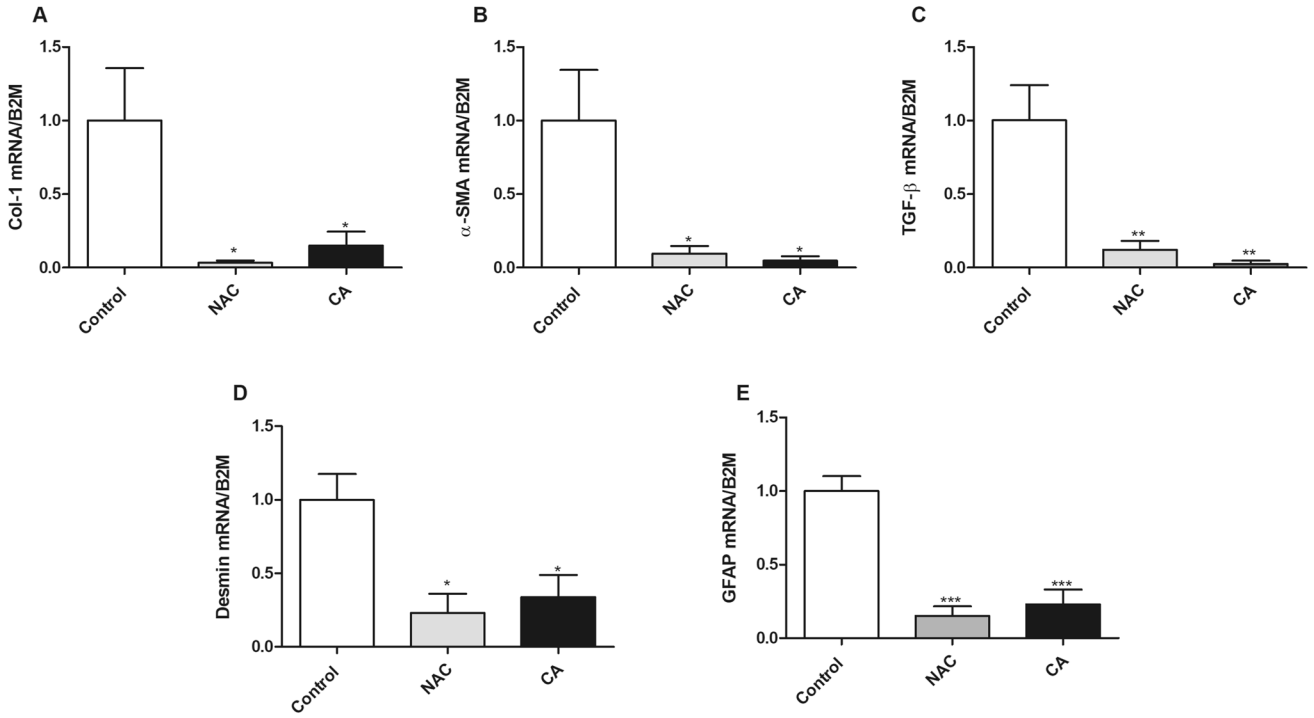

Fig. 9 Effect of CA on the expression of profibrotic genes in GRX cells after 72 h of treatment. Relative mRNA expression of **A** COL-1, **B** α-SMA, **C** TGF-β, **D** Desmin, and **E** GFAP. B2M was used as an internal control. Results are target gene/B2M, and data represent mean ± SD ($n = 4$). *$p < 0.05$, **$p < 0.01$ and ***$p < 0.001$ in comparison to the control

Effect of CA on the expression of extracellular matrix genes

Considering the ability of CA to induce the production of lipid droplets in GRX cells, we have evaluated the gene expression of pro-fibrotic genes, such as Col-1 (Fig. 9A) α-SMA (Fig. 9B), TGF-β (Fig. 9C), Desmin (Fig. 9D) and Glial fibrillary acidic protein (GFAP; Fig. 9E). We observed that CA decreased the gene expression of all fibrotic markers.

Discussion

The main cells present in the liver are the hepatocytes, hepatic stellate cells, and Kupffer cells, arranged in a hexagonal lobe, creating unique physiology and thus performing a wide range of functions necessary to maintain homeostasis. However, as a result of the action of external factors (viruses, alcohol) liver function can be largely compromised, leading to life-threatening conditions. HF is a regenerative process induced by chronic liver injury and is characterized by increased collagen deposition and replacement of healthy and functional liver tissue by non-functional scar tissue.

The treatments available to date are ineffective and most anti-fibrosis drugs are still in the stage of preclinical research, including drugs for chronic liver disease and liver fibrosis induced by different etiologies (Rahman et al. 2021). Therefore, in terms of therapeutic options for HF, there is still a need for more effective treatments. In the present study, we have evaluated the antifibrotic potential of the main phenolic compounds found in the ethanol extract of MP and its fractions. Among all the phenolics tested, CA presented the best results, as the treatment was able to reduce cell growth without inducing cell necrosis. We have also tried to test if the antiproliferative effect was by inducing apoptosis. Our results, evaluated by flow cytometry, showed that the treatment does not induce apoptosis or necrosis, corroborating the findings of the LDH enzyme assay. In order to confirm that the decrease in proliferation was not involved in cell apoptosis, we have evaluated the expression of the BAX gene (BCL-2-associated X protein) which, when inserted into the mitochondrial membrane, induces the release of cytochrome C and cell death by apoptosis (Edlich 2018). Our results have also shown that the BAX gene was not altered, confirming data obtained by flow cytometry and that the antiproliferative effect of CA is not through apoptosis.

Another mechanism leading to decreased cell proliferation is cell cycle arrest. Therefore, cellular cycle pathways were investigated. Cell cycle arrest occurs in response to many different triggers, including DNA damage, telomere dysfunction, oncogene activation, and organelle stress, and has been

shown to exhibit a finite capacity for cell division before entering an irreversible growth arrest known as replicative senescence (Di Micco et al. 2021). In antifibrotic therapy, a decrease in HSC proliferation is a promising approach to treatment. In order to explore this aspect, the study aimed to examine the CA potential in modulating the gene expression of cyclin-dependent kinase inhibitor p53, p21, p16, and p27 RNA. CA treatment showed an increase in the p53 gene expression, and, consequently, increased p21 expression. However, CA treatment did not increase p16 or p27 expression levels. Thus, the findings on the treatment with CA suggest that the decrease in cell proliferation is due to a process of cell cycle arrest by the activation of the p53/p21 genes.

Cyclin-dependent kinases (CDKs) play an essential role in regulating cell cycle progression, allowing the transition between different phases. Its activation depends on molecules that are synthesized and degraded during the cell cycle. As cell cycle regulators, their inhibition ensures that diseased cells do not undergo cell division, thus preventing them from proliferating and breaking a growth cycle (Li et al. 2021). For this reason, we have evaluated CCND1, CDK2, CDK4, and CDK6 genes. The treatments showed inhibition of cyclin D1 expression levels (CCND1), as well as CDK2, CDK4, and CDK6, which are important cell cycle regulators in cell proliferation and growth (Besson et al., 2008). These results suggest a strong correlation between the decrease in cell numbers and the induction of cell cycle arrest, which is being triggered by the p53 and p21 pathways, key regulators in cell cycle progression.

The quiescent, non-activated stellate cells, have in their cytoplasm drops of fat, mainly composed of vitamin A. When these cells are activated during the fibrotic process, they become elongated (myofibroblast) and lose drops of fat (Mendes Ouri et al. 2018). One of the ways to treat liver fibrosis is by deactivating stellate cells. From the ORO assay, we are able to visualize (under phase contrast microscopy) the lipid deposits in the cytoplasm of GRX cells. Our results showed that CA-treated GRX cells lost their activated myofibroblast appearance and accumulate lipid droplets inside the cells compared to the control. Thus, treatment with CA has an antiproliferative effect and the ability to deactivate HSCs, transforming the fibroblastic phenotype into quiescent cells.

The PPAR nuclear receptor subfamily regulates several metabolic processes, including fatty acid β-oxidation, glucose utilization, cholesterol transport, energy balance, and adipocyte differentiation. The PPAR-γ is a nuclear receptor that modulates the activation and reduces cell proliferation of HSCs and, therefore, reduces the expression of α-SMA, collagen, and TGF-β (Alatas et al. 2020). Thus, we have investigated the expression of PPAR-γ mRNA and observed that the expression of the PPAR-γ gene was increased with the treatment, suggesting the possible restoration of the quiescence HSC phenotype. NAC did not alter the expression of PPAR-γ mRNA, which is in agreement with previous literature, since its effect is mainly related to the expression of PPAR-α (Calzadilla et al. 2011).

In addition, after hepatocytes are injured, HSCs are activated and acquire a myofibroblastic phenotype in an effect driven by TGF-β and cytokines. This process leads to increased expression of contractile filaments, such as α-SMA, and ECM proteins, such as collagen (Troeger et al. 2012; Alatas et al. 2020). In addition to activating ECM proteins, activated HSCs strongly increase expression of desmin, expressed in all muscle types, including myofibroblasts, and GFAP, also noted in HSC-derived myofibroblasts, in comparation with quiescent HSCs and other non-parenchymal cells in the liver, especially in advanced fibrosis (Zhang et al. 2018; Kim et al. 2018a). Thus, we have evaluated the effects of CA treatment on the activation of ECM genes (α-SMA, Col-1, and TGF-β) as well as desmin and GFAP, demonstrating that CA was able to reduce its expression, further supporting the evidence of the deactivation of HSCs.

Conclusion

Currently, phytochemicals such as phenolic compounds may present great importance both in the prevention and treatment of diseases due to their antioxidant, antiproliferative, anti-inflammatory, and antineoplastic properties. Our in vitro study showed that CA reduces the proliferation of HSCs without inducing cell membrane damage. Furthermore, results suggest that the antiproliferative effect is related to the induction of cell cycle arrest, mediated by the upregulation of the p53 and p21 pathways. This upregulation may lead to the inhibition of CDKs, triggering a possible arrest of the cell cycle. Our results also demonstrate that the treatments tested were able to modulate the phenotype of activated HSCs by activating PPAR-γ and decreasing profibrotic genes, as well as increasing the production of lipid droplets, which is another marker of the deactivation of HSCs returning to their quiescent stage. Finally, our data present in vitro evidence to support a potential therapeutic effect of CA in the treatment of liver fibrosis.

Author contribution JOR and ERS conceived and planned this project. MSB performed all experiments. BPC, GHV, and DM helped in phenotypic reversal and gene expression experiments. KHA performed the flow cytometry experiments. RMS helped during the gene expression experiments as well as in writing the manuscript. MSB analyzed the data and wrote the manuscript with review and contributions from JOR, ERS, and MFD. All authors approved the final manuscript.

Funding This study was funded by the Coordenação de Aperfeiçoamento de Pessoal de Nível Superior (CAPES/Brazil; Financial Code 001), through a fellowship for the first author, and by National Council for Scientific and Technological Development (CNPq/Brazil) (Grant#311424/2018–0). License for Research on Brazil's Biodiversity,

CNPq#010852/2014–0 and Sistema Nacional de Gestão do Patrimônio Genético e do Conhecimento Tradicional Associado–SISGEN# ABAD620.

Availability of data and materials When requested, the authors provided the data and materials used for the development of the manuscript.

Declarations

Ethical approval Not applicable.

Competing interests The authors declare no competing interests.

References

Alatas FS, Matsuura T, Pudjiadi AH et al (2020) Peroxisome proliferator-activated receptor gamma agonist attenuates liver fibrosis by several fibrogenic pathways in an animal model of cholestatic fibrosis. Pediatr Gastroenterol Hepatol Nutr 23:346. https://doi.org/10.5223/pghn.2020.23.4.346

Bassiony H, Sabet S, Salah El-Din TA et al (2014) Magnetite nanoparticles inhibit tumor growth and upregulate the expression of P53/P16 in Ehrlich solid carcinoma bearing mice. PLoS ONE 9:e111960. https://doi.org/10.1371/journal.pone.0111960

Basso B de S, de Mesquita FC, Dias HB et al (2019) Therapeutic effect of Baccharis anomala DC. extracts on activated hepatic stellate cells. EXCLI J 18:91–105. https://doi.org/10.17179/excli2018-1696

Besson A, Dowdy SF, Roberts JM (2008) CDK inhibitors: cell cycle regulators and beyond. Dev Cell 14:159–169. https://doi.org/10.1016/j.devcel.2008.01.013

Calzadilla P, Sapochnik D, Cosentino S et al (2011) N-acetylcysteine reduces markers of differentiation in 3T3-L1 adipocytes. Int J Mol Sci 12:6936–6951. https://doi.org/10.3390/ijms12106936

Cha H, Lee S, Lee JH, Park J-W (2018) Protective effects of p-coumaric acid against acetaminophen-induced hepatotoxicity in mice. Food Chem Toxicol 121:131–139. https://doi.org/10.1016/j.fct.2018.08.060

Cheng D, Chai J, Wang H et al (2021) Hepatic macrophages: key players in the development and progression of liver fibrosis. Liver Int 41:2279–2294. https://doi.org/10.1111/liv.14940

Darzynkiewicz Z, Bedner E, Smolewski P (2001) Flow cytometry in analysis of cell cycle and apoptosis. Semin Hematol 38:179–193. https://doi.org/10.1016/S0037-1963(01)90051-4

David N de, Mauro M de O, Gonçalves CA et al (2014) Gochnatia polymorpha ssp. floccosa: bioprospecting of an anti-inflammatory phytotherapy for use during pregnancy. J Ethnopharmacol 154:370–379. https://doi.org/10.1016/j.jep.2014.04.005

de Moraes GV, Da Silveira MA, de Oliveira PD (2019) Genus Moquiniastrum (Asteraceae): overview of chemical and bioactivity studies. Curr Bioact Compd 15:377–398. https://doi.org/10.2174/1573407214666180524094146

de Souza BB, Haute GV, Ortega-Ribera M et al (2021) Methoxyeugenol deactivates hepatic stellate cells and attenuates liver fibrosis and inflammation through a PPAR-ɣ and NF-kB mechanism. J Ethnopharmacol 280:114433. https://doi.org/10.1016/j.jep.2021.114433

Di Micco R, Krizhanovsky V, Baker D, d'Adda di Fagagna F (2021) Cellular senescence in ageing: from mechanisms to therapeutic opportunities. Nat Rev Mol Cell Biol 22:75–95. https://doi.org/10.1038/s41580-020-00314-w

Edlich F (2018) BCL-2 proteins and apoptosis: recent insights and unknowns. Biochem Biophys Res Commun 500:26–34. https://doi.org/10.1016/j.bbrc.2017.06.190

Ghatei N, Nabavi AS, Toosi MHB et al (2017) Evaluation of bax, bcl-2, p21 and p53 genes expression variations on cerebellum of BALB/c mice before and after birth under mobile phone radiation exposure. Iran J Basic Med Sci 20:1037–1043. https://doi.org/10.22038/IJBMS.2017.9273

Ginès P, Krag A, Abraldes JG et al (2021) Liver cirrhosis. Lancet 398:1359–1376. https://doi.org/10.1016/S0140-6736(21)01374-X

Guarneire GJ, Lima NM, Carli GP, et al (2021) Ethnobotanical assessment in protected area from Brazilian Atlantic Forest. Res Soc Dev 10:e15310413714. https://doi.org/10.33448/rsd-v10i4.13714

Higashi T, Friedman SL, Hoshida Y (2017) Hepatic stellate cells as key target in liver fibrosis. Adv Drug Deliv Rev 121:27–42. https://doi.org/10.1016/j.addr.2017.05.007

Khomich O, Ivanov AV, Bartosch B (2019) Metabolic hallmarks of hepatic stellate cells in liver fibrosis. Cells 9:24. https://doi.org/10.3390/cells9010024

Kim S-E, Park JW, Kim M-J et al (2018a) Accumulation of citrullinated glial fibrillary acidic protein in a mouse model of bile duct ligation-induced hepatic fibrosis. PLoS ONE 13:e0201744. https://doi.org/10.1371/journal.pone.0201744

Kim W, Lim D, Kim J (2018b) p -coumaric acid, a major active compound of Bambusae Caulis in Taeniam, suppresses cigarette smoke-induced pulmonary inflammation. Am J Chin Med 46:407–421. https://doi.org/10.1142/S0192415X18500209

Kisseleva T, Brenner D (2021) Molecular and cellular mechanisms of liver fibrosis and its regression. Nat Rev Gastroenterol Hepatol 18:151–166. https://doi.org/10.1038/s41575-020-00372-7

Koopman R, Schaart G, Hesselink MK (2001) Optimisation of oil red O staining permits combination with immunofluorescence and automated quantification of lipids. Histochem Cell Biol 116:63–68. https://doi.org/10.1007/s004180100297

Kumar P, Nagarajan A, Uchil PD (2018) Analysis of cell viability by the lactate dehydrogenase assay. Cold Spring Harb Protoc 2018:pdb.prot095497. https://doi.org/10.1101/pdb.prot095497

Lee M, Rho HS, Choi K (2019) Anti-inflammatory effects of a P-coumaric acid and kojic acid derivative in LPS-stimulated RAW264.7 macrophage cells. Biotechnol Bioprocess Eng 24:653–657. https://doi.org/10.1007/s12257-018-0492-1

Li C, Lee S, Lai W et al (2021) Cell cycle arrest and apoptosis induction by Juniperus communis extract in esophageal squamous cell carcinoma through activation of p53-induced apoptosis pathway. Food Sci Nutr 9:1088–1098. https://doi.org/10.1002/fsn3.2084

Limeiras SMA, Oliveira BC, Pessatto LR et al (2017) Effects of Moquiniastrum polymorphum ssp floccosum ethnolic extract on colorectal carcinogenesis induced by 1,2-dimethylhydrazine. Genet Mol Res 16. https://doi.org/10.4238/gmr16019518

Liu X, Xu J, Rosenthal S et al (2020) Identification of lineage-specific transcription factors that prevent activation of hepatic stellate cells and promote fibrosis resolution. Gastroenterology 158:1728-1744.e14. https://doi.org/10.1053/j.gastro.2020.01.027

Martins GG, Lívero FA dos R, Stolf AM et al (2015) Sesquiterpene lactones of Moquiniastrum polymorphum subsp. floccosum have antineoplastic effects in Walker-256 tumor-bearing rats. Chem Biol Interact 228:46–56. https://doi.org/10.1016/j.cbi.2015.01.018

Mendes Ouri FGDO, Caruso PB, Da Silva GV et al (2018) Antifibrotic effect of Pluchea sagitallis (Lam.) cabrera aqueous extract in grx cell lineage. Int J Phytomedicine 10:30. https://doi.org/10.5138/09750185.1832

Piornedo R dos R, de Souza P, Stefanello MÉA et al (2011) Anti-inflammatory activity of extracts and 11,13-dihydrozaluzanin C from Gochnatia polymorpha ssp. floccosa trunk bark in mice. J Ethnopharmacol 133:1077–1084. https://doi.org/10.1016/j.jep.2010.11.040

Plano SA, Baidanoff FM, Trebucq LL et al (2021) Redox and antioxidant modulation of circadian rhythms: effects of nitroxyl, N-acetylcysteine and glutathione. Molecules 26. https://doi.org/10.3390/molecules26092514

Rahman MM, Shahab NB, Miah P et al (2021) Polyphenol-rich leaf of Aphanamixis polystachya averts liver inflammation, fibrogenesis and oxidative stress in ovariectomized Long-Evans rats. Biomed Pharmacother 138:111530. https://doi.org/10.1016/j.biopha.2021.111530

Roychoudhury S, Sinha B, Choudhury BP et al (2021) Scavenging properties of plant-derived natural biomolecule para-coumaric acid in the prevention of oxidative stress-induced diseases. Antioxidants 10:1205. https://doi.org/10.3390/antiox10081205

Stepanenko AA, Sosnovtseva AO, Valikhov MP et al (2022) Superior infectivity of the fiber chimeric oncolytic adenoviruses Ad5/35 and Ad5/3 over Ad5-delta-24-RGD in primary glioma cultures. Mol Ther Oncolytics 24:230–248. https://doi.org/10.1016/j.omto.2021.12.013

Strober W (2001) Trypan blue exclusion test of cell viability. In: Current Protocols in Immunology. John Wiley & Sons, Inc., Hoboken, NJ, USA

Teratake Y, Kuga C, Hasegawa Y et al (2016) Transcriptional repression of p27 is essential for murine embryonic development. Sci Rep 6:26244. https://doi.org/10.1038/srep26244

Troeger JS, Mederacke I, Gwak G et al (2012) Deactivation of hepatic stellate cells during liver fibrosis resolution in mice. Gastroenterology 143:1073-1083.e22. https://doi.org/10.1053/j.gastro.2012.06.036

Tsochatzis EA, Bosch J, Burroughs AK (2014) Liver cirrhosis. Lancet 383:1749–1761. https://doi.org/10.1016/S0140-6736(14)60121-5

Weiskirchen R, Tacke F (2016) Liver fibrosis: from pathogenesis to novel therapies. Dig Dis 34:410–422. https://doi.org/10.1159/000444556

Zhang C-Y, Yuan W-G, He P et al (2016) Liver fibrosis and hepatic stellate cells: Etiology, pathological hallmarks and therapeutic targets. World J Gastroenterol 22:10512. https://doi.org/10.3748/wjg.v22.i48.10512

Zhang D, Zhuang R, Guo Z et al (2018) Desmin- and vimentin-mediated hepatic stellate cell-targeting radiotracer 99m Tc-GlcNAc-PEI for liver fibrosis imaging with SPECT. Theranostics 8:1340–1349. https://doi.org/10.7150/thno.22806